Chinese Science Bulletin

Raman scattering and photoluminescence of Fe-doped ZnO nanocantilever arrays

ZHANG Bin, ZHOU ShaoMin†, WANG HaiWei & DU ZuLiang

Key Laboratory for Special Functional Materials, Henan University, Kaifeng 475004, China

Single crystalline Fe-doped ZnO nanocantilever arrays have been synthesized by thermal evaporating amorphous Zn-Fe-C-O composite powder. The characterizations of composition, structure and phonon spectrum properties of the nanocantilevers have been performed. Arrays of uniform, perfectly aligned and single-crystal nanowires have been observed by electron microscopy. The results of the X-ray photo-electric spectra and the Raman spectrum provide the evidence that Fe is incorporated into the ZnO lattice at Zn site. Abnormally, the room temperature UV emission band of Fe-doped ZnO nanocantilevers disappears and the green one has a large red-shift, and the intensity of the green emission is strongly quenched because the Fe^{3+} enters the ZnO crystal lattice.

semiconductor, doped, nanoarrays, photoluminescence

As a wide band gap (3.37 eV) semiconductor, ZnO is of interest for low-voltage and short wavelength (green or green/blue) electro-optical devices such as light emitting diodes and laser devices[1−12]. Up to date, quite a few interesting nanostructure arrays of ZnO including nanowires, nanonails and nanocombs have been synthesized via a vapor-phase process. The arrays have become an important issue for the more diverse range of applications. However, fabricating arrays of nanostructure including nanocantilevers (NCs) and nanocombs is a crucial step toward realization of functional nanosystems, and still represents a significant challenge in the field of nanoscale sciences[3−11]. Recently, many papers have reported fabrication of ZnO NC arrays or nanocombs[3−11]. For example, Yang's research group[2,3] reported on room-temperature ultraviolet nanowire nanolasers and dendritic nanowire ultraviolet laser array. Wang and his co-workers[4,5] synthesized ZnO nanocantilever arrays. However, reports of Fe-doped ZnO NCs and phonon spectrum properties have been limited though our group has synthesized Cd-doped ZnO NCs[9]. As far as we know, doping in semiconductor with selective elements offers an effective approach to adjust the electrical, optical and magnetic properties, which is crucial for practical applications[11−20]. Recently, our group has reported on doping ZnO[1,16−19], GaN[13,21] and CdS nanowires[15], as well as controlled their optical properties[1,13,16−19,21]. Fe^{3+} as an excellent candidate impurity for synthesizing diluted magnetic semiconductors, attracts increasing attention in the physics, material and chemistry fields. Due to its potential technological applications in emerging field of spin-based electronics, many groups have studied the magnetic and optical properties of Fe-doped ZnO films[22−24]. However, the manufacture and photoluminescence (PL) of Fe-doped ZnO NC arrays have not been reported. In this work, we synthesized Fe-doped ZnO NC arrays and studied their phonon spectrum properties. The X-ray diffraction (XRD) patterns and the Raman scattering spectrum of the as-obtained samples reveal the contraction of the lattice constants with Fe^{3+} entering ZnO crystal lattice.

Received October 11, 2007; accepted January 11, 2008
doi: 10.1007/s11434-008-0247-z
†Corresponding author (email: smzhou@henu.edu.cn)
Supported by the National Basic Research Program of China (Grant No. 2007CB616911) and the Program for Science & Technology Innovation Talents in Universities of Henan Province (HASTIT)

1 Experimental

Samples of Fe-doped ZnO NCs were synthesized via a vapor-phase process using amorphous Zn-Fe-C-O composite powder, obtained by a sol-gel method, as starting materials. $Zn(NO_3)_2 \cdot 6H_2O$ and $Fe(NO_3)_3 \cdot 9H_2O$ were dissolved in deionized water (Fe/Zn=2%, mol), and then appropriate amounts of citric acid, ethylene glycol were added. This solution was stirred until it became transparent, it was then allowed to form a sol at 353 K, and polymerized to form a gel at 423 K. The solid resin was pre-pyrolyzed at 673 K for 1 h in a crucible with a lid, in order to decompose the organic materials, and to give the amorphous precursor of Zn-Fe-C-O composite powder. The resulting amorphous precursor was ground, and then placed in a ceramic boat. Subsequently, the ceramic boat was put into a horizontal tube furnace. Si substrates were put on top of the ceramic boat to collect samples. The Fe-doped ZnO NCs were finally synthesized under N_2 (99.99%) flow rate of 50 sccm for 1 h at a temperature of about 1173 K. The products were studied and analyzed by X-ray diffraction (XRD, X'pert MRD-Philips diffractometer, Holland), scanning electron microscopy (SEM, JEOL JSM-5600LV, Japan), transmission electron microscopy (TEM, JEOL 2010, Japan), X-ray photo-electric spectrum (XPS, Axis Ultra, U.K.), Raman spectroscopy (Renishaw microscopic confocal Raman spectrometer, RW-1000, U.K.), and room temperature photoluminescence (RTPL, SPEX F212, USA).

2 Results and discussion

Figure 1(a) and (b) shows two typical SEM images of the Fe-doped ZnO NCs. Unlike those NCs of previous reports[3−5,8,9], our nanowire arrays have uniform diameters and are evenly distributed on one side of the stem with a periodicity of 50 nm. The typical diameters of the teeth are in the range of 40−50 nm and lengths up to 1 μm. As shown in Figure 1(a) and (b), each array usually contains several tens of perfectly aligned and evenly spaced nanowires with almost constant diameter and spacing. Figure 1(c) shows a typical TEM image of the as-synthesized Fe-doped ZnO samples. These hierarchically ordered nanowire arrays are monolithically single crystalline as evidenced by selected area electron diffraction pattern (SAED) (Figure 1(d)). The comb backbone grows along $[2\bar{1}\bar{1}0]$, its top/bottom surfaces are $(01\bar{1}0)$, and these nanoteeth grow along [0001]. High-resolution TEM (HRTEM) was applied to characterize microstructures of a single NC (Figure 1(e)). In the HRTEM image, perfect and continuous lattice fringes reveal that Fe^{3+} ions were adulterated into the crystal lattice of ZnO and formed a hexagonal single crystal structure. Based on analysis of HRTEM, SAED, and XRD, the lattice spacing (0002 for 0.26 nm) of the un-doped ZnO NC is larger than that (0002 for 0.251 nm) of Fe-doped ZnO NC, which is induced by doping Fe^{3+} ion into the ZnO crystal lattice (the Fe ion (0.55 Å) has smaller ionic radii than Zn ion (0.74 Å)).

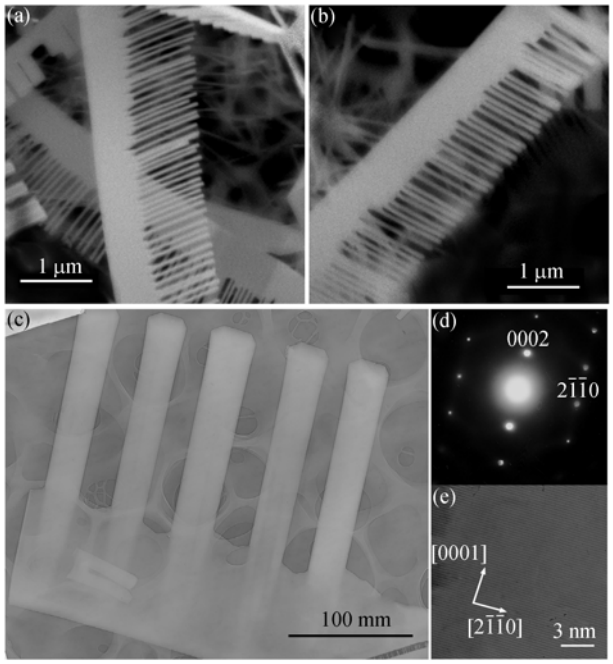

Figure 1 (a), (b) Representative SEM images of the ZnO NCs; (c) TEM image of Fe-doped ZnO NCs; (d) the corresponding electron diffraction pattern, showing that the NC-stem direction is $[2\bar{1}\bar{1}0]$, while the teeth direction is [0001]; (e) HRTEM image of the Fe-doped ZnO NC.

Figure 2(a) shows XRD patterns of the as-synthesized Fe-doped ZnO NCs where the diffraction peaks can be indexed to a hexagonal wurtzite structured ZnO. The inset in Figure 2(a) presents two high-resolution XRD spectra of Fe-doped (marked with gray) and un-doped (marked with black) samples. The XRD peaks located at 34.4° and 34.52° (as shown in the inset) are for un-doped and Fe-doped ZnO NCs, respectively. The shift of XRD peaks of Fe-doped NCs is about 0.12°, indicating that Zn cations have been successfully substituted with smaller Fe cations (Fe^{3+}), which is in good agreement with the analysis of HRTEM.

We employed high-resolution XPS spectra for the chemical composition analysis and electric structure

analysis of Fe-doped ZnO NCs. XPS spectra were recorded using monochromatized Al *K*α radiation (1486.8 eV) and C1s (*E*=284.8 eV) level served as the internal standard (Figure 2(b)-4). In Figure 2(b)-1, two peaks of $Zn2p_{3/2}$ and $Zn2p_{1/2}$ are exhibited at 1021.2 eV and 1044.4 eV, respectively. The main binding energy peak of O1s (530.1 eV) is believed to be the lattice oxygen whereas the high binding energy peak (531.7 eV) is the absorbed oxygen (Figure 2(b)-2). As shown in Figure 2(b)-3, the binding energies of the $Fe2p_{3/2}$ and $Fe2p_{1/2}$ are about 704 eV and 717.3 eV, respectively. The two peaks clearly separate, which indicates that all Fe is typical of Fe^{3+} in the oxidation state. The Fe content is estimated to be about 3% (atom) from the analysis of XPS spectra. The binding energy values of Zn2p and O1s are well according with those of the bulk ZnO, which indicates that the valency of Zn is +2 in the Fe-doped ZnO NCs.

The Raman scattering spectrum of Fe-doped ZnO NCs is presented in Figure 3(a). For un-doped ZnO, the 330 cm^{-1} and the 379 cm^{-1} frequency are respectively for the second-order vibration mode and A_1 (TO) mode. The phonon frequency of E_2 (high) and E_1 (LO) modes are 436 cm^{-1} and 578 cm^{-1}. Compared with those of un-doped ZnO, Fe-doped ZnO has the classical Raman modes at 336, 384, 438, 538 cm^{-1}, and an additional mode at 634 cm^{-1}. Up to now, there are many reports of similar additional vibration modes in ZnO. Bundesmann et al.[22] observed the vibration mode at 644 cm^{-1} in Fe-, Sb-, Al-, Ga-, and Li-doped ZnO films and proposed that this additional mode is related to intrinsic host-lattice defects. In our experiment, the additional mode appears after doping, which may be due to Fe^{3+} occupation at Zn^{2+} sites or defects in the NCs.

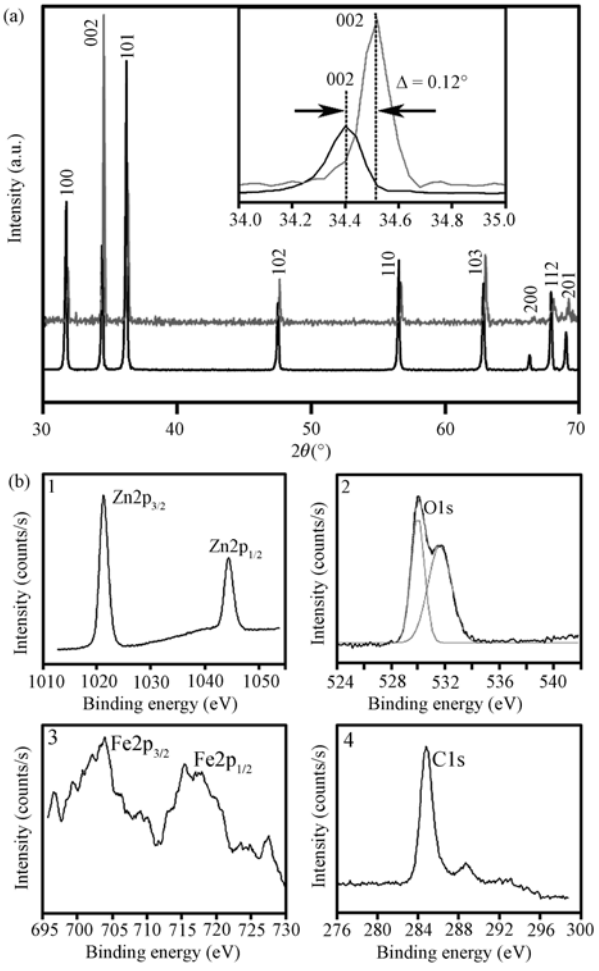

Figure 2 (a) Full-range XRD pattern taken from the Fe-doped ZnO NCs (gray line) and un-doped ZnO NCs (black line). The inset plots the (002) peaks in a magnified scale, the (002) peak shift is around 0.12°. (b) High-resolution (HR) XPS spectra of Fe-doped ZnO NCs. 1, Zn2p; 2, O1s; 3, Fe2p; 4, C1s.

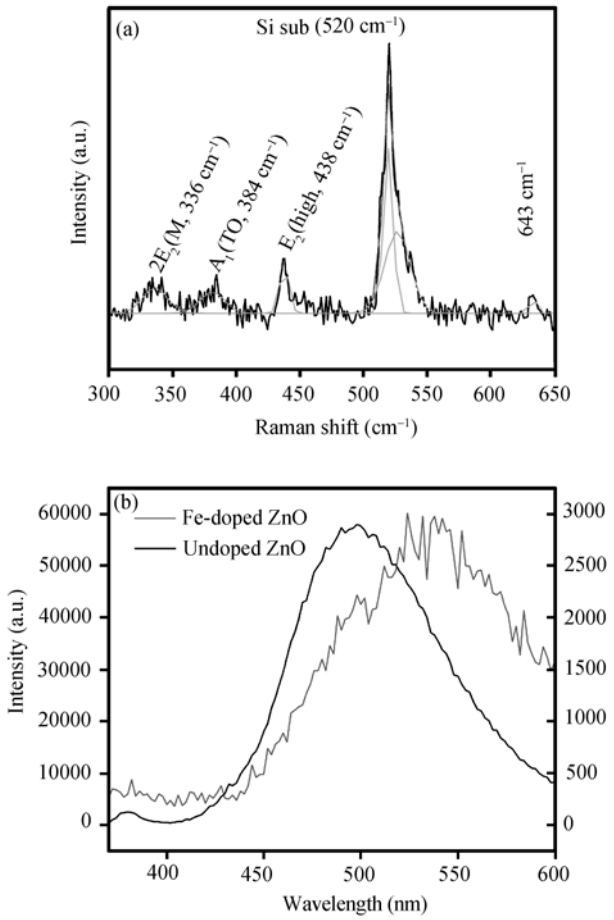

Figure 3 (a) Raman scattering spectra of Fe-doped ZnO NCs using He-Ne laser at 632.8 nm line; (b) two PL spectra of the as-produced un-doping and doping ZnO NCs based on the Xe lamp (330 nm) as the excitation light source.

Based on the same wavelength scale, Figure 3(b) shows room temperature photoluminescence (RTPL) spectra of a bulk quantity un-doped and Fe-doped ZnO samples. A broad green emission band centered (as indicated with gray) at ~536 nm is from the Fe-doped ZnO NCs. Compared with RTPL of un-doped samples (as marked with black), the green emission band of the Fe-doped ZnO NCs shows a large red-shift and its intensity is strongly quenched with the Fe entering the ZnO crystal lattice. The results are compatible with previous reports on Fe-doped ZnO nanocrystals and Mn-doped ZnO thin films[23,24]. In addition, for the red shift, this is probably due to the increasing number of PL centers of elemental iron[1,25].

Here, we believe the formation of the Fe-doped ZnO NCs is controlled by a vapor-solid (VS) process. Ma et al.[26] explained the growth processes of wurtzite CdSe "forming nanoribbons first, teeth growing then". We suggest that the growth process can be divided into two stages: firstly there form the NC-stems {forming nucleation and growing in $[2\bar{1}\bar{1}0]$ direction}, and then the NC-teeth are created (slower growth in [0001] direction by a faceted epitaxial growth process)[27]. The detailed growth process of Fe-doped ZnO NC is illustrated by SEM images (Figure 4). As shown in Figure 4(a)—(f), under Fe catalysis, the carbon atoms can directly reduce composite oxides into Zn(Fe) and form vapors. Again, these vapors can react with O_2 to form eutectoid of ZnFeO nanoparticles, and then form like-wire or like-rod nanostructures as demonstrated by Figure 4(a). Due to the existence of diffusion gradient, thermal perturbation (on the surface of the nanowire) forms inhomogeneous nucleus. Once any sporadic prominencies occur on the solid-vapor interface, the NC-teeth can project toward preferential surfaces of (0001), which results in the faceted epitaxial growth of the NC-teeth in [0001] direction (Figure 4(b) and (c)). Continuous offering with the evaporated Zn(Fe) source and elemental oxygen, the teeth of NCs mentioned above become more and longer (Figure 4(d)), the adjacent teeth link together, and ultimately the like-ribbon nanostructure forms, of which the counterpart data are shown in Figure 4(e) and (f). In the future, one of our focuses is to produce more detailed and substantiated data to confirm the growth mechanism of the NCs.

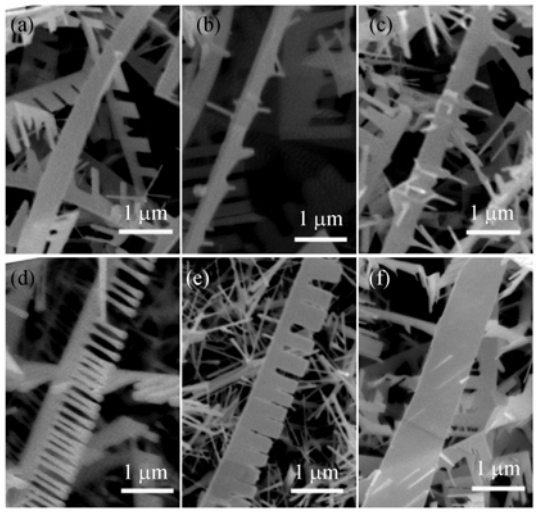

Figure 4 SEM images of the Fe-doped ZnO NCs, showing its growth process.

3 Conclusions

In summary, the Fe-doped ZnO NCs are synthesized by a two-step routine. Such synthesized NCs in our experiment may indicate a new way to assemble uniform semiconductor nanowires into highly ordered one-dimensional nanoscale arrays. The growth mechanism of Fe-doped ZnO NCs is believed to be conventional VS mechanism. Microstructure analysis shows that Fe-doped ZnO NCs are single crystalline phase. Detections of XRD, HRTEM, XPS, and Raman spectrum indicate that Fe^{3+} substitutes into ZnO lattice at Zn^{2+} site (not a straightforward mixed compound). The simple friendly environment doping technique can be used to fabricate other morphology-controlled doping semiconductor NCs or nanocombs and may be viable for large-scale applications of nanotechnologies.

1 Zhou S, Zhang X, Meng X, et al. The fabrication and optical properties of highly crystalline ultra-long Cu-doped ZnO nanowires. Nanotechnology, 2004, 15: 1152—1155
2 Huang M, Mao S, Feick H, et al. Room-temperature ultraviolet nanowire nanolasers. Science, 2001, 292: 1897—1899
3 Yan H, He R, Johnson J, et al. Dendritic nanowire ultraviolet laser array. J Am Chem Soc, 2003, 125: 4728—4729
4 Wang Z, Kong X, Zuo J. Induced growth of asymmetric nanocantilever arrays on polar surfaces. Phys Rev Lett, 2003, 91: 185502—185505
5 Wang Z, Kong X, Ding Y, et al. Semiconducting and piezoelectric oxide nanostructures induced by polar surfaces. Adv Funct Mater, 2004, 14: 943—956
6 Liu F, Cao P, Zhang H, et al. Controlled self-assembled nanoaeroplanes, nanocombs, and tetrapod-like networks of zinc oxide. Nanotechnology, 2004, 15: 949—952

7 Shen G, Bando Y, Lee C. Growth of self-organized hierarchical ZnO nanoarchitectures by a simple In/In2S3 controlled thermal evaporation process. J Phys Chem B, 2005, 109: 10779—10785
8 Pan Z, Mahurin S, Dai S, et al. Nanowire array gratings with ZnO combs. Nano Lett, 2005, 5: 723—727
9 Zhou S, Meng X, Zhang X, et al. Large-scale fabrication and characterization of Cd-doped ZnO nanocantilever arrays. Micron, 2005, 36: 55—59
10 Wang J, Sun X, Wei A, et al. Zinc oxide nanocomb biosensor for glucose detection. Appl Phys Lett, 2006, 88: 233106—233108
11 Yuhas B, Fakra S, Marcus M, et al. Probing the local coordination environment for transition metal dopants in zinc oxide nanowires. Nano Lett, 2007, 7: 905—909
12 Yuhas B, Zitoun D, Pauzauskie P, et al. Transition-metal doped zinc oxide nanowires. Angew Chem, Int Ed, 2006, 45: 420—423
13 Zhou S. Fabrication and PL of Al-doped gallium nitride nanowires. Phys Lett A, 2006, 57: 374—377
14 Song Y, Wang P, Zhang X, et al. Magnetism and luminescence evolution due to nitrogen doping in manganese-gallium oxide nanowires. Phys Lett A, 2006, 351: 302—307
15 Zhou S. Fabrication and optical properties of Sb-doped CdS nanowires. Mater Lett, 2007, 61: 119—122
16 Zou K, Qi X, Duan X, et al. Sb-induced bicrystal ZnO nanobelts. Appl Phys Lett, 2005, 86: 013103—013105
17 Zhou S, Zhang X, Meng X, et al. Preparation and photoluminescence of Sc-doped ZnO nanowires. Physica E, 2005, 25: 587—591
18 Zhou S, Zhang X, Meng X, et al. Synthesis and optical properties of Pb-doped ZnO Nanowires. Phys Stat Sol, 2005, 202: 405—410
19 Zhou S, Zhang X, Meng X, et al. Fabrication of large-scale ultra-fine Cd-doped ZnO nanowires. Mater Res Bull, 2006, 41: 340—346
20 He J, Lao C, Chen L, et al. Large-scale Ni-doped ZnO nanowire arrays and electrical and optical properties. J Am Chem Soc, 2005, 127: 16376—16377
21 Zhou S. Near UV photoluminescence of Hg-doped GaN nanowires. Physica E, 2006, 33: 394—397
22 Bundesmann C, Ashkenov N, Schubert M, et al. Raman scattering in ZnO thin films doped with Fe, Sb, Al, Ga, and Li. Appl Phys Lett, 2003, 83: 1974—1976
23 Norberg N, Kittilstved K, Amonette J, et al. Synthesis of colloidal Mn2+:ZnO quantum dots and high-TC ferromagnetic nanocrystalline thin films. J Am Chem Soc, 2004, 126: 9387—9398
24 Wang Y, Thomas P, Brien P. Optical properties of ZnO nanocrystals doped with Cd, Mg, Mn, and Fe ions. J Phys Chem B, 2006, 110: 21413—21415
25 Zhou S, Feng Y, Zhang L. Growth and optical characterization of large-scale crystal CdxZn1̃xS whiskers via vapor reaction. J Cryst Growth, 2003, 252: 1—3
26 Ma C, Ding Y, Moore D, et al. Single-crystal CdSe nanosaws. J Am Chem Soc, 2004, 126: 708—709
27 Chen Y, Jiang J, He Z, et al. Growth mechanism and characterization of ZnO microbelts and self-assembled microcombs. Mater Lett, 2005, 59: 3280—3283